Modeling and identification on nonlinear saturable and reverse-saturable absorptions of gold nanorods using femtosecond *Z*-scan technique

Rui Wang (王 睿)[1], Yingshuai Wang (王英帅)[1], Dan'ao Han (韩丹翱)[1], Chuantao Zheng (郑传涛)[1], Jiyan Leng (冷吉燕)[2], and Han Yang (杨 罕)[1*]

[1]*State Key Laboratory on Integrated Optoelectronics, College of Electronic Science and Engineering, Jilin University, Changchun 130012, China*

[2]*First Hospital of Jilin University, Changchun 130021, China*

[*]*Corresponding author: Yanghan@jlu.edu.cn*

Received March 5, 2012; accepted April 13, 2012; posted online August 3, 2012

An improved *Z*-scan analysis approach is proposed by establishing and solving the saturable absorption (SA) and reverse-SA (RSA) models, respectively. Near-infrared femtosecond *Z*-scans are carried out on the synthesized gold nanorods (NRs) possessing the average length of 46 nm using a femtosecond laser operated at the wavelength of 800 nm, which is close to the peak position of longitudinal surface plasmon resonance (SPR) (710 nm) of gold NRs. At lower input intensity of less than 400 GW/cm^2, the normalized transmission exhibits only SA phenomenon; however, when it exceeds 400 GW/cm^2, both SA and RSA are observed. By using the presented *Z*-scan modeling and theory, the three-photon absorption (3PA) is identified in the material, and the 3PA cross-section is determined to be 1.58×10^{-71} cm^{6}s^2.

OCIS codes: 190.0190, 190.4400.

doi: 10.3788/COL201210.101902.

Generally speaking, nonlinear absorption, which includes saturable absorption (SA), reverse-SA (RSA), multi-photon absorption (MPA), and free carrier absorption (FCA), possesses various applications[1−3]. For example, SA materials are applied extensively in laser pulse compression[4], and optical bistability, among others, whereas RSA, 2PA, and MPA materials are applied in two-photon fluorescence microscopy and imaging[5−7], 3D optical storage, microfabrication[8−10], up-conversion lasing[11−13], and optical limiting[14]. Therefore, identifying different nonlinear absorption processes is important, especially for the acquisition of corresponding nonlinear absorption parameters, such as the saturable intensity for saturable absorber, 2PA cross-section for 2PA material, and MPA coefficient for MPA material.

The *Z*-scan technique, which was first proposed by Sheik-Bahae *et al.*[15], was widely used for characterizing the optical nonlinearities of a sample with simple apparatus, as well as relatively high sensitivity. In Ref. [15], 2PA was analyzed as an example, where the normalized energy transmittance was expressed as a summation of numerical evaluations, thereby obtaining the 2PA coefficient . With the research of diverse materials, other nonlinear and simultaneously appearing absorption processes have been observed from open aperture (OA) *Z*-scan traces[16−19]. Therefore, distinguishing the nonlinear absorption effects and acquiring the related nonlinear parameters for the materials possessing more than one nonlinear absorption effect are important.

Consequently, in this letter, we establish an improved *Z*-scan technique model for charactering a nonlinear, optical, and thin absorber with SA, RSA (including 2PA, 3PA, and other MPA), or both processes. We divide the absorption term into two parts, SA and RSA, and the solution of each phenomenon is derived individually. First, for SA, by using the similar main principle Gu *et al.*[20], the computational difficulty is reduced by utilizing the improved Adomian operator. The first seven terms of normalized transmittance polynomial are identified, which are sufficient for characterizing the complicated nonlinear absorption process. After acquiring the saturable intensity from the first step, the numerical expression of RSA cross-section is achieved through the analytical polynomial expressions of reverse-saturable *Z*-scan trace[21]. Gold nanorods (NRs)[22−24] are utilized as the sample due to their complicated nonlinear absorption process. By using the proposed SA and RSA models and their related solutions, the nonlinear absorption parameters are determined by best fitting the theoretical curve (represented by nonlinear absorption parameters) to the experimental data. To the best of our knowledge, we are the first to present a quantitative analysis of the nonlinear absorption process of gold NRs, although similar material regarding this phenomenon has been reported previously[25]. The good agreement between the theoretical curve and the experimental results verify that our modeling and solutions can efficiently identify and evaluate both saturable intensity and MPA coefficients, which can also be adapted to the OA *Z*-scam analysis on other SA or RSA materials.

Considering the beam propagation in a thin nonlinear absorber, the optical intensity loss is governed by

$$\frac{\mathrm{d}I}{\mathrm{d}z'} = -\alpha(I)\,I, \tag{1}$$

where z' and I are the propagation distance and optical intensity inside the nonlinear sample, respectively, and $\alpha(I)$ is the absorption coefficient dependent on the intensity. Supposing that both SA and RSA exist simulta-

neously, the absorption coefficient is

$$\alpha(I) = \frac{\alpha_0}{1 + I/I_s} + \beta I + \alpha_2 I^2 + \alpha_3 I^3 + \alpha_4 I^4 + \cdots, \tag{2}$$

where I_s is the saturable intensity.

Equation (1) is a nonlinear ordinary differential equation, and is usually difficult to solve using the existing approach. This difficulty may be one of the reasons most groups only conduct qualitative analysis. For obtaining the solution from Eq. (1), we divide the absorption coefficients into two parts: SA absorption term and RSA absorption term.

When we consider only the SA, the SA absorption can be modeled by

$$\alpha(I) = \frac{\alpha_0}{1 + I/I_s}, \tag{3}$$

where α_0 is the linear absorption coefficient. Generally speaking, explicit analytical solutions of the intensity transmitted through nonlinear absorbers are difficult to obtain. For the SA model, the intensity distribution at the exit surface of the nonlinear sample expressed by I^{out} can be written as

$$I^{\text{out}} = I^{\text{in}} - \int_0^L f(I)\,\mathrm{d}z', \tag{4}$$

where $f(I) = \frac{\alpha_0 I}{1+I/I_s}$, L is the length of the saturable absorber, and I^{in} is the input optical intensity at the entrance face of the saturable absorber.

According to the Adomian method[26], I^{out} can also be represented as a series

$$I^{\text{out}} = \sum_{k=0}^{\infty} I_k, \tag{5}$$

and the nonlinear term $f(I)$ is decomposed as

$$f(I) = \sum_{k=0}^{\infty} A_k, \tag{6}$$

where A_k are polynomials in $I_1, I_2, \cdots, I_k$, called Adomian polynomials, obtained by

$$A_k = \frac{1}{k!} \frac{\partial^k f(\sum_{i=0}^{k} \lambda^k I_k)}{\partial \lambda^k} |_{\lambda=0}. \tag{7}$$

Here, we use a modification of Adomian polynomials to accelerate the rapid computing efficiency compared with the standard Adomain method. Substituting Eq. (5) into Eq. (3) and combining Eqs. (3) with (4), we have

$$\sum_{k=0}^{\infty} I_k = I^{\text{in}} - \int_0^L \sum_{k=0}^{\infty} A_k \mathrm{d}z'. \tag{8}$$

By making the 0th component $I_0 = I^{\text{in}}$, one can obtain the other components I_k by the recurrence formula

$$I_{k+1} = -\int_0^L A_k \mathrm{d}z'. \tag{9}$$

Adding all terms of I_k, obtaining the exact solution I^{out} from Eq. (1) is simple:

$$I^{\text{out}} = I^{\text{in}}\Big[1 + \sum_{k=1}^{\infty} \frac{(-\alpha_0 L)^k g_k(\eta)}{(1+\eta)^{2k-1}}\Big], \tag{10}$$

where $\eta = I^{\text{in}}/I_s$. The first seven terms of $g_i(\eta)$ $(i = 1, 2, \cdots, 7)$ are obtained as

$$g_1(\eta) = 1, \tag{11a}$$

$$g_2(\eta) = 1, \tag{11b}$$

$$g_3(\eta) = 1 - \eta, \tag{11c}$$

$$g_4(\eta) = 1 - 3\eta + \eta^2, \tag{11d}$$

$$g_5(\eta) = 1 - 6\eta + 6\eta^2 - \eta^3, \tag{11e}$$

$$g_6(\eta) = 1 - 10\eta + 20\eta^2 - 10\eta^3 + \eta^4, \tag{11f}$$

$$g_7(\eta) = 1 - 13\eta + 37\eta^2 - 32\eta^3 + 7\eta^4. \tag{11g}$$

Assuming a Gaussian beam propagates through a sample along the z direction, the optical intensity at the incident plane of the sample I^{in} is

$$I^{\text{in}} = \frac{I_0(t)}{1 + x^2} \exp\left[-\frac{2r^2}{\omega^2(x)}\right], \tag{12}$$

where $\omega^2(x) = \omega_0^2\left(1 + x^2\right)$, $x = z/z_0$, z is the sample position, ω_0 is the radius of the beam waist, and z_0 is Rayleigh length. Here, $I_0(t) = I_{00}\exp[-(t/t_0)^2]$ is the instantaneous intensity of the Gaussian beam, where I_{00} is the on-axis peak intensity.

According to the principle of the OA Z-scan, the analytical solution of the normalized transmittance is

$$\begin{aligned} T(x,t) &= \frac{\int_0^{\infty} I^{\text{out}}(x,t)\, r\mathrm{d}r}{\mathrm{e}^{-\alpha_0 L}\int_0^{\infty} I^{\text{in}} r\mathrm{d}r} \\ &= \mathrm{e}^{\alpha_0 L}\left[1 + \sum_{k=1}^{\infty} (-\alpha_0 L)^k q_k(\rho)\right], \end{aligned} \tag{13}$$

where $\rho = I_0(t)/\left[I_s\left(1 + x^2\right)\right]$, and the first seven terms of $q_k(\rho)$ $(k = 1, 2, \cdots, 7)$ are

$$q_1(\rho) = \frac{\ln(1+\rho)}{\rho}, \tag{14a}$$

$$q_2(\rho) = \frac{1}{2\rho}\left[1 - \frac{1}{(1+\rho)^2}\right], \tag{14b}$$

$$q_3(\rho) = \frac{1}{6\rho}\left[1 - \frac{1-2\rho}{(1+\rho)^4}\right], \tag{14c}$$

$$q_4(\rho) = \frac{1}{12\rho}\left[1 - \frac{1-6\rho+3\rho^2}{(1+\rho)^6}\right], \tag{14d}$$

$$q_5(\rho) = \frac{1}{20\rho}\left[1 - \frac{1 - 12\rho + 18\rho^2 - 4\rho^3}{(1+\rho)^8}\right], \tag{14e}$$

$$q_6(\rho) = \frac{1}{30\rho}\left[1 - \frac{5}{(1+\rho)^6} + \frac{60}{(1+\rho)^7} - \frac{210}{(1+\rho)^8} + \frac{280}{(1+\rho)^9} - \frac{126}{(1+\rho)^{10}}\right], \tag{14f}$$

$$q_7(\rho) = \frac{1}{264\rho}\left[7 - \frac{231}{(1+\rho)^8} + \frac{1760}{(1+\rho)^9} - \frac{4620}{(1+\rho)^{10}} + \frac{5064}{(1+\rho)^{11}} - \frac{1980}{(1+\rho)^{12}}\right]. \tag{14g}$$

The normalized energy transmittance for a temporal Gaussian pulse can be yielded by

$$T(x) = \frac{1}{\sqrt{\pi}}\int_{-\infty}^{\infty} T(x,t)e^{-\frac{t^2}{\tau^2}}\mathrm{d}t. \tag{15}$$

Then, we consider the RSA terms only, the solution of Eq. (1) is easily obtained from various methods. Although we can still use the Adomian method, the scope of the results of these methods is smaller than when using the polynomial method. Therefore, we adopt the polynomial method in Ref. [21]. The Z-scan of the n-photon absorber thus has the following form:

$$T_{n\mathrm{PA}}(x) = 1 - \frac{1}{n^{3/2}}\frac{\alpha_n I_0^{n-1} L_{\mathrm{eff}}^{(n)}}{(1+x^2)^{n-1}} \text{ (for Gaussian beams)}, \tag{16}$$

where $L_{\mathrm{eff}}^{(n)} = \{1 - \exp[-(n-1)\alpha_0 L]\}/(n-1)\alpha_0$ is the effective sample length related to the nPA. One can apply Eq. (16) to identify the n-photon RSA process manifesting itself in a Z-scan.

Gold NRs were prepared by using a seed-mediated wet chemical approach with a quaternary ammonium surfactant cetyltrimethylammo-nium bromide (CTAB)[27]. The ratio aspect of gold NRs ranged from 1.5 to 10, for which the surface plasmon absorption (SPA) was between 600 and 1 300 nm. The CTAB (99%) and $NaBH_4$ (99%) were both purchased from Sigma-Aldrich and used without further purification. The ascorbic acid, $HAuCl_4$, and $AgNO_3$ were ordered from China. Deionized water was used in all the experiments. The seed and growth solutions below for the preparation of the old NRs were prepared as described.

7.5 mL CTAB solution (0.100 mol/L) was mixed with 0.25 mL $HAuCl_4$ (0.001 mol/L) under stirring. Next, 1.0 ml deionized water and 0.60 mL $NaBH_4$ (0.010 mol/L) were added, which resulted in the formation of a brownish yellow solution. The solution was kept at 25 °C under stirring.

After the seed solution was kept for 2 h, 200 ml CTAB (0.10 mol/L) was added to 10 ml $HAuCl_4$ (0.001 mol/L) solution at room temperature. Mixing $AgNO_3$ and $HAuCl_4$ at the concentration of micromolar scale will definitely result in the formation of AgCl precipitates. Then, 1.8 ml $AgNO_3$ (0.01 mol/L) was added. After the gentle mixing of the solution, 1.1 ml of 0.1 mol/L ascorbic acid was also added. After a period of time, the growth solution changed from dark yellow to colorless. The final step was the addition of 0.24 ml of the seed solution to the growth solution. The color of the solution gradually changed within 15–20 min. The temperature of the growth medium was kept constant at 30 °C. After 6 h, the gold NRs can be obtain; the solution concentration was 8×10^{-9} mol/L.

In the insert of Fig. 1, the transmission electron microscopy (TEM) image clearly shows the presence of gold NRs with an average length of 46 nm. The absorption spectra of the gold NRs dissolved in water were measured with a UV-spectrophotometer (UV-1700, Shimadzu), as illustrated in Fig. 1, which clearly showed two surface plasmon resonance (SPR) peaks. The first small SPR peak at 580 nm is due to the transverse mode perpendicular to the gold NRs, whereas the second strong SPR peak at 710 nm is due to the length area of the gold NRs, which gives rise to the longitudinal mode of SPR. These huge SPR peaks, which may often be expected to exhibit SA phenomenon, can be attributed to the conduction band transition of s-p electron[25].

The nonlinear optical properties of gold NRs dissolved in water were investigated with the femtosecond OA Z-scan technique[6,28]. The excitation source was a Ti sapphire regenerative amplifier (1 k-10 Hz, 120 fs, Spectra-Physics Spitfire Pro) operated at the wavelength of 800 nm near the peak position of longitudinal SPR (710 nm) of gold NRs. The laser pulses were focused into a 1-mm-thick quartz cuvette using a lens with a focal length of 150 mm. The beam waist was approximately 20 μm.

The irradiance-intensity-dependent behaviors with 800-nm incident wavelength obtained from the OA Z-scan measurement of gold NRs are shown in Fig. 2(a). At relatively lower excitation intensity, the gold NRs reveal SA behavior. In addition, as the intensity increases, the gold NRs exhibit an additional RSA behavior. Figure 2(b) shows the further characteristics of the sample with simultaneous appearance of SA and RSA. We can see that the OA Z-scan traces (circle line) change along with the increase of the input intensity. When I_{00} <400 GW/cm^2, the normalized transmission exhibits only SA phenomenon; whereas, when I_{00} > 400 GW/cm^2, both SA and RSA appear. These intensity-dependent transmittance curves (when the sample is located at z=0) can be used to identify different nonlinear absorption process.

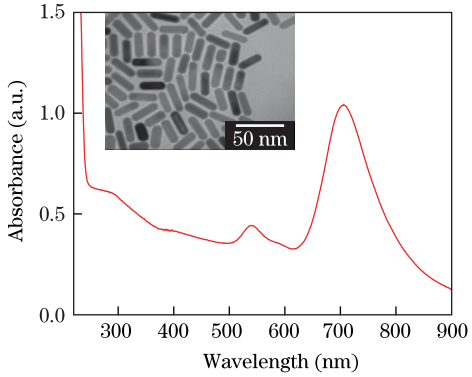

Fig. 1. Absorption spectra and TEM image (inset) of gold NRs.

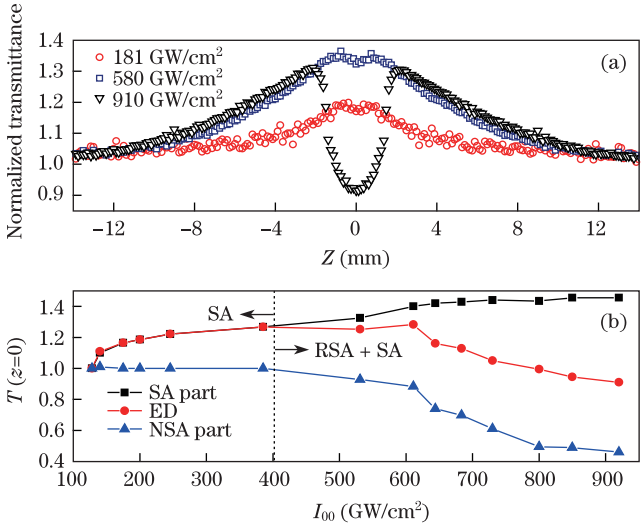

Fig. 2. (a) Normalized Z-scan results of the gold NRs at different excitation intensities, and (b) dependence of $T(0)$ on I_{00} for the gold NRs. ED: experimental data.

Similar nonlinear SA and RSA optical effects exist widely in metal nanoparticles. Generally, SA behavior is ascribed to ground state plasmon bleaching, and RSA is ascribed to excited state absorption, interband transition, and FCA. Despite these assumptions, in practical application, the issue of concern is the nonlinear optical parameters of the materials. In the following, by using the proposed theoretical SA and RSA models, the optical nonlinearities of gold NRs are analyzed and related parameters are derived through numerical fitting and processing on experimental data.

In our experiment, the Gaussian laser beam at 800 nm was focused by a lens with a focal length of 150 mm. The focused beam waist was estimated to be 20 μm, and the Rayleigh range was $Z_0 = 1.4324$ mm, which guaranteed the thin medium conditions. The experimental data at different irradiation intensities of I_{00}= 245.8, 385.4, 530.87, and 683.6 GW/cm^2 are shown in Fig. 3. In Figs. 3(a) and (b), under lower irradiation intensities, only SA is observed, whereas in Figs. 3(c) and (d), both SA and RSA are exhibited. These results are in accordance with the results in Fig. 2(b).

In order to utilize our models to exactly analyze the nonlinear absorption process, a more-universal situation is considered (Fig. 3(c)). The data processing procedure is performed as follows (see Fig. 4):

(1) Determine the SA intensity I_s. Adjust the parameter (I_s) in Eq. (15) to find a trace that best fits the SA part of the experimental data (open circle line) shown in Fig. 4(a). The optimized value is I_s= 32 GW/cm^2. Thus, one can obtain the theoretical SA part, as shown by the solid line in Fig. 4(a).

(2) Determine the absorption process and find the related absorption coefficient. Remove the theoretical SA part from the experimental data, and then can derive the RSA part (open circle line shown in Fig. 4(b)). Using the polynomial method[20](Eq. (16)), we can strive to make the optimal 2PA curve, 3PA curve, and 4PA curve fit the experimental data. The results are shown in Fig. 4(b). Because the 3PA curve has the best accordance with the experimental data, the nonlinear absorption phenomenon is identified as 3PA, and the corresponding 3PA coefficient is $\alpha_3 = 4.3 \times 10^{-5}$ cm^3/GW^2.

(3) Calculate both theoretical SA and RSA results. Combine the theoretical SA results obtained from step (1) and the RSA results from step (2). The total theoretical absorption results (solid line) are shown in Fig. 4(c), which agree well with the experimental data (open circle line).

The fitting results (solid line) using similar steps are shown in Figs. 3(a), (b), and (d). The optical parameters of the four irradiation intensities for the sample are listed in Table 1.

The 3PA absorption cross-section for the gold NRs in water was determined by[29]

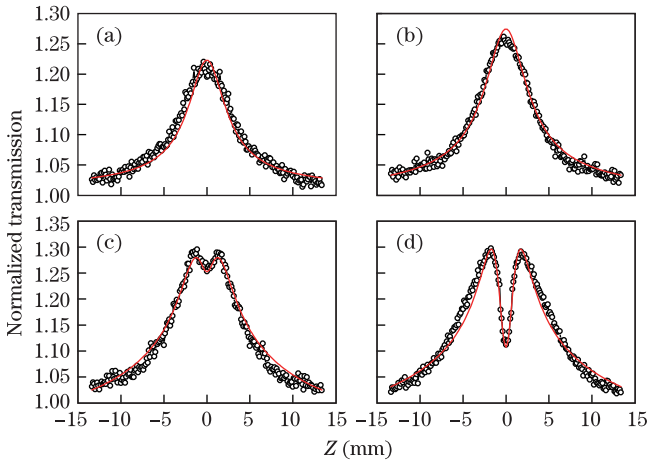

Fig. 3. OA Z-scans of the gold NRs measured at different irradiation intensities of (a) 245.8, (b) 385.4, (c) 530.87, and (d) 683.6 GW/cm^2. The solid lines represent the best-fit curves calculated by using the improved Z-scan analytical theory, and the open circles represent the ED.

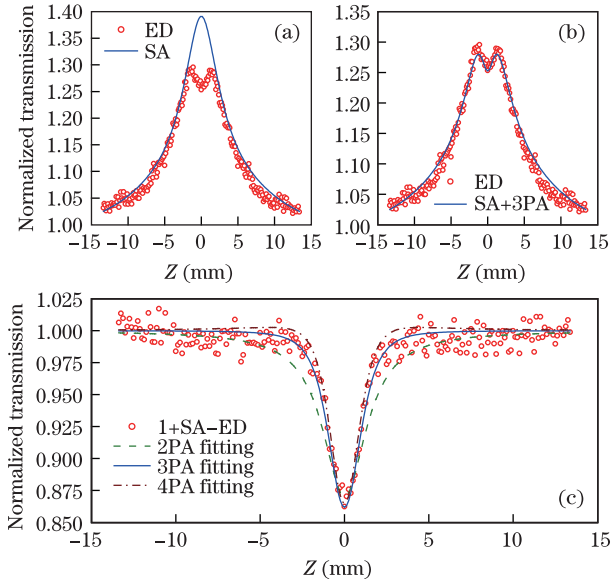

Fig. 4. Data processing procedure for identifying the nonlinear absorption process and related optical parameters: (a) determining the SA intensity I_s; (b) determining the absorption process; (c) calculating both theoretical SA and RSA results.

Table 1. Optical Parameters of the Four Irradiation Intensities in Fig. 3

Figure/ Absorption Process	I_{00} (GW/ cm^2)	$\alpha_0 L$	α_3 (cm^3/ GW^2)	I_s (GW/ cm^2)
(a)/SA	245.8	0.3	0	26
(b)/SA	385.4	0.33	0	26
(c)/SA+3PA	530.87	0.435	4.3×10^{-5}	32
(d) /SA+3PA	683.6	0.435	1.05×10^{-4}	36

$$\sigma_3 = \frac{\gamma}{N_A d_0 \times 10^{-3}}(h\nu)^2, \tag{17}$$

where σ_3 is the molecular 3PA cross-section in units of cm^{6}s^2, N_A is the Avogadro's number, d_0 is the molar concentration, and $h\nu$ is the photon energy of the input light beam. In the experiment, the 3PA cross-section for gold NRs in water was 1.58×10^{-71} cm^{6}s^2.

In conclusion, an improved Z-scan model for characterizing the nonlinear absorption process is established. By dividing the absorption terms into two separate parts, the solutions of SA model and RSA model are derived. The computational difficulty is reduced by the improved Adomian operator, and the results are sufficient for characterizing the complicated nonlinear absorption process. In order to check the proposed model and solution, Z-scan measurements are carried out on the prepared gold NRs, and both absorption process and related nonlinear optical parameters are determined. The results of gold NRs show that, at lower input intensity of $I_{00} < 400$ GW/cm^2, the normalized transmission exhibits only SA phenomenon, whereas, when $I_{00} > 400$ GW/cm^2, both SA and RSA become evident. The 3PA process is identified through data processing, and the 3PA cross-section is 1.58×10^{-71} cm^{6}s^2. The good agreement between the theoretical curve and experimental results prove that our modeling and solutions can efficiently identify and evaluate both saturable intensity and MPA coefficients, and can also be adapted to the OA Z-scan analysis on other SA or RSA materials.

This work was supported by the National Natural Science Foundation of China under Grant Nos. 61077002, 61107021, 91123029, and 61077066.

References

1. K. D. Belfield, D. J. Hagan, E. W. V. Stryland, K. J. Schafer, and R. A. Negres, Org. Lett. **1,** 1575 (1999).
2. H.-H. Fang, Q.-D. Chen, J. Yang, H. Xia, Y.-G. Ma, H.-Y. Wang, and H.-B. Sun, Opt. Lett. **35,** 441 (2010).
3. W. Denk, J. H. Strickler, and W. W. Webb, Science **248,** 73 (1990).
4. Y. X. Fan, J. L. He, Y. G. Wang, S. Liu, H. T. Wang, and X. Y. Ma, Appl. Phys. Lett. **86,** 101103 (2005).
5. I. L. Medintz, H. T. Uyeda, and E. R. Goldman, Nat. Mat. **4,** 435 (2005).
6. P. Kumbhakar, M. Chattopadhyay, R. Sarkar, and U. Chatterjee, Chin. Opt. Lett. **9**, 101902 (2011).
7. F. Liu, Y. Li, Q. Xing, C. Wang, M. Hu, L. Chai, and C. Wang, Chin. Opt. Lett. **9,** 10201 (2011).
8. D. Wu, Y. B. Zhao, S. Z. Wu, Y. F. Liu, H. Zhang, S. Zhao, J. Feng, Q. D. Chen, D. G. Ma, and H. B. Sun, Opt. Lett. **36,** 2635 (2011).
9. B. B. Xu, Z. C. Ma, L. Wang, R. Zhang, L. G. Niu, Z. Yang, Y. L. Zhang, W. H. Zheng, B. Zhao, Y. Xu, Q. D. Chen, H. Xia, and H. B. Sun, Lab. Chip. **11,** 3347 (2012).
10. Y. L. Sun, W. F. Dong, R. Z. Yang, X. Meng, L. Zhang, Q. D. Chen, and H. B. Sun, Angew. Chem. Int. Ed. **51,** 1558 (2012).
11. G. S. He, R. Signorini, and P. N. Prasad, Appl. Opt. **37,** 5720 (1998).
12. Q. D. Chen, H. H. Fang, B. Xu, J. Yang, H. Xia, F. P. Chen, W. J. Tian, and H. B. Sun, Appl. Phys. Lett. **94,** 201113 (2009).
13. H. H. Fang, B. Xu, Q. D. Chen, R. Ding, F. P. Chen, J. Yang, R. Wang, and H. B. Sun, IEEE J. Quantum Electron. **46,** 1775 (2010).
14. J. E. Ehrlich, X. L. Wu, I.-Y. S. Lee, Z.-Y. Hu, H. Rockel, S. R. Marder, and J. W. Perry, Opt. Lett. **33,** 1843 (1997).
15. M. Sheik-Bahae, A. A. Said, T. H. Wei, D. J. Hagan, and E. W. Van Stryland, IEEE J. Quantum Electron. **26**, 760 (1990).
16. Y. C. Gao, X. R. Zhang, Y. L. Li, H. F. Liu, Y. X. Wang, Q. Chang, W. Y. Jiao, and Y. L. Song, Opt. Commun. **251,** 429 (2005).
17. S. V. Rao, N. K. M. N. Srinivas, and D. N. Rao, Chem. Phys. Lett. **361,** 439 (2002).
18. C. Zheng, X. Y. Ye, S. G. Cai, M. J. Wang, and X. Q. Xiao, Appl. Phys. B **101,** 835 (2010).
19. Y. H. Lee, Y. L. Yan, L. Polavarapu, and Q. H. Xu, Appl. Phys. Lett. **95,** 023105 (2009).
20. B. Gu, Y. X. Fan, J. Wang, J. Chen, J. P. Ding, H. T. Wang, and B. Guo, Phys. Rev. A **73,** 065803 (2006).
21. B. Gu, X. Q. Huang, S. Q. Tan, M. Wang, and W. Ji, Appl. Phys. B **95,** 375 (2009).
22. B. B. Xu, Z. C. Ma, H. Wang, X. Q. Liu, Y. L. Zhang, X. L. Zhang, R. Zhang, H. B. Jiang, and H. B. Sun, Electrophoresis **32,** 3378 (2011).
23. Y. W. Hao, H. Y. Wang, Y. Jiang, Q. D. Chen, K. Ueno, W. Q. Wang, H. Misawa, and H. B. Sun, Angew. Chem. Int. Ed. **50,** 7824 (2011).
24. Y. Jiang, H. Y. Wang, H. Wang, B. R. Gao, Y. W. Hao, Y. Jin, Q. D. Chen, and H. B. Sun, J. Phys. Chem. C **115,** 12636 (2011).
25. H. I. Elim, J. Yang, and J. Y. Lee, Appl. Phys. Lett. **88,** 083107 (2006).
26. A. M. Wazwaz, Appl. Math. Comput. **102,** 77 (1999).
27. N. R. Jana, L. Gearheart, and C. J. Murphy, Adv. Mater. **13,** 1389 (2001).
28. R. Wang, L. Y. Pan, X. D. Xia, D. A. Han, J. Q, and H. Yang, Chemical Journal of Chinese Universities **33,** 149 (2012).
29. J. H. Liu, Y. L. Mao, M. J. Huang, Y. Z. Gu, and W. F. Zhang, J. Phys. Chem. A **111,** 9013 (2007).